1972

The effect of gravity on nucleate pool boiling of water.

Smith, Gibson Peter.

Monterey, California. Naval Postgraduate School

THE EFFECT OF GRAVITY ON NUCLEATE POOL BOILING OF WATER

Gibson Peter Smith

NAVAL POSTGRADUATE SCHOOL

Monterey, California

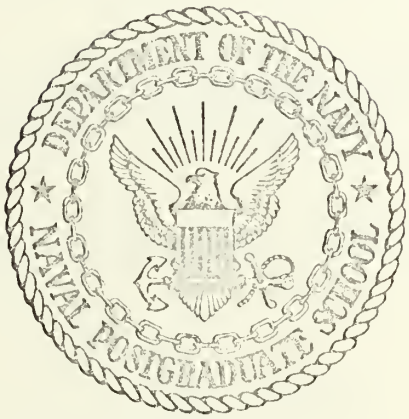

THESIS

THE EFFECT OF GRAVITY ON
NUCLEATE POOL BOILING OF WATER

by

Gibson Peter Smith

Thesis Advisor: P. J. Marto

December 1972

Approved for public release; distribution unlimited.

The Effect of Gravity on Nucleate Pool Boiling of Water

by

Gibson Peter Smith
Lieutenant Commander, United States Navy
B.S., United States Naval Academy, 1959

Submitted in partial fulfillment of the
requirements for the degree of

MASTER OF SCIENCE IN MECHANICAL ENGINEERING

from the

NAVAL POSTGRADUATE SCHOOL
December 1972

ABSTRACT

The effect of gravity levels up to 400 times the local gravity value (a/g) was experimentally investigated in a copper, rotating, cylindrical boiler. Heat flux levels up to 80,000 BTU/hr-ft^2 were reached.

Observed improvement in heat transfer at low heat flux values with increasing gravity levels confirmed the results of previous investigations. At high heat flux values, a consistent trend was not observed. With increasing gravity levels, some data indicated a decrease in heat transfer while other data indicated an increase in heat transfer. Changes in heat transfer with variation of the liquid annulus thickness was noted.

TABLE OF CONTENTS

TABLE OF SYMBOLS

A	surface area of evaporator, ft^2
C_L	specific heat of liquid, BTU/Lbm - °F
g_c	conversion factor, 32.17 ft-Lbm/Lbf-sec^2
g	acceleration of gravity, ft/sec^2
h	heat transfer coefficient, BTU/hr-ft^2-°F
h_{fg}	enthalpy of vaporization, BTU/Lbm
k	thermal conductivity of copper, BTU/hr-ft-°F
L	length of evaporator, ft
$\dot{m}$	coolant mass flow rate, Lbm/hr
m	slope of thermal conductivity curve, BTU/hr-ft-$°F^2$
p	pressure, Lbf/ft^2
P_{satw}	evaporator wall saturation pressure, Lbf/ft^2
P_{atm}	atmospheric pressure, Lbf/ft^2
Q	heat transfer rate, BTU/hr
Q/A	heat flux, BTU/hr-ft^2
$q"$	heat flux, BTU/hr-ft^2
r	radial distance, ft
r_a	radius to liquid annulus, ft
r_c	radius to thermocouple location, ft
r_i	inner evaporator wall radius, ft
T	temperature, °F
T_B	fluid bulk temperature, °F
Tc	thermocouple temperature, °F
To	zero degrees, °F
T_{satw}	saturation temperature at evaporator wall, °F
T_{satv}	saturation temperature in vapor space, °F

T_{wall} evaporator inner wall temperature, °F

ΔT temperature difference, °F

Greek

ρ_L density of liquid, Lbm/ft^3

ρ_V density of vapor, Lbm/ft^3

w angular velocity, rad/sec

β volume coefficient of expansion, 1/°R

ν kinematic viscosity, ft^2/sec

σ surface tension of vapor-liquid interface, Lbf/ft

Dimensionless Numbers

$Pr = \frac{Cp\rho\nu}{k}$ Prandtl Number

$Gr = \frac{g\beta\Delta TL^3}{\nu^2}$ Grashof Number

I. INTRODUCTION

The study of the effect of increased gravity levels on nucleate pool boiling has been underway for approximately eleven years. This study has been pursued because boilers and vapor-generation devices are being extensively revised because of new requirements for their use in spaceflight applications and in the widening use of nuclear reactors as energy sources. These boilers are required to operate at high heat flux levels and under variable gravity levels. The study of the effects of high gravity levels on the boiling phenomenon may also lead to a new understanding of the boiling heat transfer mechanism.

The objective of this investigation was to obtain improved data on nucleate boiling of water at high heat flux levels and at gravity levels up to 400 times the local gravity value (a/g). This was done in order to determine if there was a significant variation in heat transfer rates in this region with gravity level change and if there was any reversal in the direction of the variation.

Costello and Tuthill [1] studied the influence of increased gravity levels of 1 to 45 a/g upon nucleate boiling heat transfer at heat flux levels between 100,000 and 200,000 BTU/hr ft^2. In this limited range of study, increased gravity levels required larger values of superheat for a constant heat flux. Heat transfer was decreased for increases in acceleration in this region.

Merte and Clark [2] studied the influence of increased acceleration, from 1 to 21 a/g, upon nucleate boiling heat transfer in saturated water. Under pool boiling conditions, they detected an acceleration effect which was dependant upon the heat flux level. For values of heat flux less than 50,000 BTU/hr ft^2, increased acceleration decreased the superheat required. At heat flux levels above 50,000 BTU/hr ft^2, increased acceleration increased the superheat required. They postulated two different modes of heat transfer to explain this; nucleate boiling and natural convection heat transfer. At low levels of heat flux, natural convection heat transfer governed heat removal and increased gravity levels enhanced heat transfer rates. At high heat flux levels, nucleate boiling heat transfer was predominant and increased gravity levels decreased heat transfer rates.

In the natural convection region Ref. [3] recommends using formula

$$Nu = C(GrPr)^m \quad , \quad 10^5 < (GrPr) < 2x10^7$$

for horizontal flat plates where C = .54, m = .25, Gr = Grashof number, Pr = Prandtl number, and Nu = Nusselt number. Grashof number = $\frac{g\beta\Delta TX^3}{\nu^2}$ and is thus directly proportional to the gravity level. This shows that as gravity level increases, heat transfer rates in the natural convection region also increase.

Adelberg [4] compared gravity forces with three other forces which also influence the heat transfer rate in nucleate boiling. These forces were bubble dynamic forces, surface tension, and forced convection induced drag. He then reviewed existing literature for experimental data which he considered relevant and compared his analysis with this data.

Later, Adelberg [5] developed three equations for heat transfer in pool nucleate boiling. The range of applicability of each equation depended upon the gravity level. From experimental data available, he concluded that his equations for low and moderate a/g levels agree favorably with the limited data available. No data was available to verify his equation for high a/g levels.

Graham and Hendricks [6] investigated the influence of acceleration upon the mechanism of heat transfer in saturated liquid boiling from 1 to 10 a/g. They demonstrated that increasing acceleration tended to shift the boiling characteristic curve in the direction of improved heat transfer rates in proportion to the 1/4 power of the difference in wall temperature and fluid bulk temperature.

Gray, Marto, and Joslyn [7] investigated heat transfer behavior in a rotating boiler using acceleration up to 200 a/g and heat fluxes up to 505,000 BTU/hr ft^2. This study confirmed that at low heat fluxes, increased acceleration increased heat transfer rates; whereas at high heat fluxes, the opposite was true. This was in agreement with previous

experimenters. The region where this crossover effect took place occurred at progressively higher heat flux levels for higher accelerations. They concluded that unresolved effects such as surface condition and aging affected the data at high heat fluxes as much as did gravity variations from 1 to 200 a/g.

Marto and Gray [8] investigated high acceleration and heat flux effects on nucleate boiling. They achieved accelerations up to 400 a/g and heat fluxes to 818,000 BTU/hr ft^2. Their results showed that for the inception of nucleate boiling from natural convection, heat flux and required wall superheat increased as acceleration increased. They also verified that at low heat fluxes, increased acceleration increased heat transfer rates. But at high heat fluxes, heat transfer rates were practically independent of acceleration variations. In this region changes in heat transfer rates were as small in magnitude as the usual scatter in experimental data.

Judd and Merte [9] studied the heat flux predictions of six different models proposed to explain the nucleate boiling phenomenon. They showed that none of the models adequately predict nucleate boiling heat flux for other than saturated boiling conditions at standard gravity. All the models predicted decreasing values of heat flux as acceleration increased. These observations suggested the omission of some mechanisms which are inoperative under standard conditions of gravity, but very sensitive to the level of subcooling and acceleration.

They presented an empirical procedure for correlating the results used in their study. Their equation for heat flux is

$$Q/A = 0.16\ Pr^{1/3}\left(\frac{g\beta k^3}{\nu 2}\right)^{1/3}\ (T_{wall}-T_B)^{4/3}\ (a/g)^{1/3}$$

$$+2.39 \times 10^{6}\ Pr^{-4.1}\ \frac{k(T_{wall}-T_B)}{\sqrt{\frac{g_c}{g}\frac{\sigma}{(e_\ell - e_v)}}}\cdot\left[C_L\frac{(T_{wall}-T_{satv})}{hfg}\right]^2$$

Metric units must be used in this equation.

The first term is the contribution of natural convection and the second term the contribution of nucleate boiling. They showed that as a/g increases, $(T_{wall}-T_B)$ decreases when both $(T_{wall}-T_{satv})$ and Q/A are constant. At low heat flux levels, the first term is important since natural convection dominates. As a/g increases, the heat flux may either increase or decrease depending upon the magnitude of $(a/g)^{1/3}$ compared to $(T_{wall}-T_B)^{4/3}$. At high heat flux levels, the first term becomes insignificant and the second term dominates. In this region Q/A will decrease with increased a/g since the $(T_{wall}-T_B)$ term decreases. This suggests that there may be a crossover region of heat flux where the effect of increasing gravity level is reversed.

II. EQUIPMENT CONFIGURATION

To conduct this high gravity nucleate boiling investigation, the boiler section of an existing rotating thermosyphon apparatus was used.

Figure 1 is a schematic diagram of the thermosyphon assembly and associated equipment. Figure 2 is a cross sectional drawing of the thermosyphon. Figure 3 is a photograph of the equipment setup in the laboratory.

The equipment was the same as that used by Woodard [10] with the following modifications. The entire thermosyphon was manufactured from pure copper stock with the exception of the two end plates of the evaporator. These were manufactured from 304 stainless steel. The grooves were designed to reduce heat transfer from the barrel of the evaporator to the end plates. The difference in the thermal conductivity of the two different materials served the same purpose in this design. The condenser end was left open to the atmosphere by removing the .25 inch threaded plug in the end section.

A. EVAPORATOR MANUFACTURE

The evaporator section was manufactured from pure copper stock and the end sections from 304 stainless steel. It had an inside diameter of 3.125 inches and an outside diameter of 3.635 inches. The length of the copper section was 3.125 inches, and when assembled the overall length was 3.75 inches. The actual heated length was 3.5 inches. The heating coil

was 11-gauge Chromel-A heater wire in a 0.1875 inch inconel sheath helically wound around the evaporator.

The procedure for bonding the stainless steel end plates to the copper section and bonding the heater wire to the evaporator was an exacting process. Its purpose was to ensure a uniform heat flux axially along the heater surface and to prevent electrical shorting between the heater wire and other components. The procedure was as follows:

1. A thin sheet of gold copper foil was tack welded to the outside evaporator surface and each end section.
2. The heater wire was wound over the gold-copper foil with gold-copper wire wound intermittently between the coils.
3. The stainless steel end plates were then pressed in place.
4. The entire assembly was brazed in a hydrogen atmospherically-controlled oven.
5. Sauereisen cement was air dried around the outside of the heater wire.
6. Asbestos insulation was wrapped around the heater wire and tied off with glass tape.

Power was supplied to the heater coils by a 130 volt D.C. source capable of delivering a maximum of 100 amperes. This power was transmitted by a brush assembly consisting of eight spring-loaded graphite brushes through two bronze collector rings to the heater wire. The bronze collector

rings were supported by twelve 0.25 inch stud bolts. Phenolic spacers were used to align the rings and to insulate the bolts from the rings.

The outside face of the evaporator was closed by two pyrex glass view ports. The inner port rested on a neoprene O-ring and was separated from the outer port by a compressed fiber gasket. A glass tube was fused to the inner port and passed through a hole in the outer port. This tube was used for evacuating and filling the system when used as a thermosyphon.

In order to measure the temperature gradient in the evaporator wall, four holes, 0.0625 inches in diameter and 2.375 inches deep, were drilled radially in the evaporator wall. Four sheathed thermocouples were inserted into these holes. The center of one hole was located 0.0625 inches from the inner wall and another hole's center was located the same distance from the outer wall. These holes were located 180 degrees apart. The remaining two holes were drilled so that their centers were 0.125 inches from the inner wall. These two holes were also located 180 degrees apart.

Due to the relative softness of copper, these holes were not drilled true, and it was thus necessary to measure the misalignment of each hole. This was done to determine the exact position of each thermocouple junction. The following procedure was used on each hole to determine its misalignment.

A 0.0625 inch diameter pin 2.5 inches in length was hardened at one end for approximately 0.5 inches to preclude any bending. This pin was inserted in the drilled hole with the hardened end outward. Protruding from the hole was a 0.125 inch section. A precision square 2.375 inches high was aligned to the edge of the drilled hole using the protruding pin end for alignment. When properly aligned, the precision square was clamped in place and the metallic alignment pin removed. Then a Tungsten heliarc electrode approximately six inches in length and 0.0625 inches in diameter was inserted into the hole. This electrode was chosen because it is manufactured to be precision straight. The misalignment between the precision square and the tungsten electrode at the top of the block was measured using precision feeler gages. Since the electrode was assumed to be perfectly straight, the misalignment of the electrode at the top of the precision square was the same as at the bottom of the drilled hole.

This procedure showed that the ends of the drilled holes were located as follows from the centerline of the evaporator: 1.610, 1.672, 1.683, and 1.770 inches, respectively. The hole nearest the inner wall was only .016 inches from the wall. A slight protrusion was visible. Due to the softness of the copper, the drilling may have caused the wall surface to bulge very slightly.

B. INSTRUMENTATION

1. Temperature Measurements

Temperature measurements were obtained from four, 30 gauge, copper-constantan thermocouples. These were inserted in 0.0625 inch diameter holes drilled 2.375 inches deep in the evaporator wall. They were sheathed in 0.0625 inches OD stainless steel tubing.

The manufacture of these thermocouples required a careful procedure. First, the outer plastic insulation was removed from the wires by using a low flame to melt the insulation. The residue was then carefully scraped from the inner wires using a surgical blade. Extreme care was used so that the insulation of the inner wires was not ruptured. This outer insulation was removed from a one foot section of each thermocouple.

Stainless steel tubing, 0.063 inches OD, was cut into lengths of approximately five inches. The stripped thermocouple wires were inserted into the tubing and the ends of the wires were soft soldered to make the junction. With this junction made, the wires were pulled back until only approximately 1/4 inch remained exposed. A coating of Conley-Weld epoxy adhesive was placed over the exposed wires and junction. Then the wires were again pulled back until only the epoxy covered junction was exposed. The epoxy was used to protect the junction and to hold the wires securely in the tube. After the epoxy had set, fine

sandpaper was used to make a smooth finish and reduce the size of the tip to that of the tubing.

The leads from the four thermocouples in the evaporator wall were brought down the outside of the condenser and through the rear condenser flange to a junction board at the end of the shaft. From the junction board, the leads went inside the main shaft to a slip ring assembly which was attached to the main shaft by a coupling.

The output from the slip rings was fed to a Hewlett-Packard 2010C Data Acquisition System. This system provided printed or visual output of the thermocouple readings.

2. Rotational Speed Measurement

The rotational speed of the evaporator was measured using a magnetic pickup and a Systron Donner Counter 1013 Series. An electronic strobe light was used as a check

3. Condenser Cooling Water Temperature Measurement

The inlet and outlet cooling water temperatures to the condenser section were measured using a Hewlett-Packard 2801A Quartz Thermometer. The uncertainty in these readings was ±.1°F.

4. Electric Power Measurement

The power into the evaporator section was measured using DC voltage and amperage meters.

5. Cooling Water Flow Rate Measurement

The cooling water flow rate to the condenser was measured using a calibrated flow rotameter. The calibration procedure for this rotameter is described in Ref. [11]. The uncertainty in these readings was ±.5%.

6. Liquid Annulus Thickness Measurement

The liquid annulus thickness was measured by a paper rule scribed in 1/16 inch marks attached to the viewing glass at the evaporator end. The uncertainty in these readings was ±.032 inches.

C. OPERATING PROCEDURE

The evaporator was filled with approximately 200 ml of distilled water using a syringe. Filling was accomplished either from the condenser end or the evaporator end thru the glass tube. When using the latter method, the glass tube was sealed after filling. Cooling water flow was then established to a 30% reading on the rotameter. The drive motor was then energized and the desired RPM established. When a liquid annulus had formed, DC power was applied to the evaporator heater. With the desired RPM and power level established, data was recorded when thermal equilibrium was established. Waiting time between data recording ranged from 5 to 15 minutes after a change in variables. The following data were recorded: RPM, a/g, power supplied to the heater, four thermocouple readings, coolant mass flow rate, temperature difference across the condenser, atmospheric pressure, and liquid annulus thickness.

Securing the machine was accomplished by first shutting off power to the evaporator heater and then shutting off the drive motor. Lastly, the cooling water was secured.

III. EXPERIMENTAL RESULTS

The original method of heat flux calculation was to use the four thermocouples installed in the evaporator wall to determine the radial temperature distribution across the evaporator wall. With this temperature distribution determined, the inside wall temperature, T_{wall}, could be computed along with the heat flux, Q/A, as described in Appendix B.

Power level was limited to 6 kilowatts. Above this level, steaming occurred from the condenser end and considerable vapor was lost to the atmosphere. The initial data run revealed that with the highest power level available, the temperature variation across the evaporator was too small to be accurately determined by the thermocouples. This was due to the high thermal conductivity of the copper evaporator, the thin wall, and the limit on the power level. The errors in the location of the thermocouple wells described in section II also contributed to the uncertainty in the thermocouple readings. Therefore this method of calculation was abandoned.

The alternate method used to calculate the evaporator wall temperature and the heat flux was to make a heat balance on the condenser section. The heat supplied to the evaporator equals the voltage times amperage supplied to the heater. The heat to the condenser section equals the heat supplied to evaporator minus convection and radiative heat losses to the atmosphere. The heat removed from the condenser section equals the heat supplied from the

evaporator section plus the heat generated by friction in the seals and bearings plus the heat generated by viscous dissipation in the coolant. These last two sources of heat generation can be combined into the heat generated due to rotation. An overall heat balance states that the heat supplied to the evaporator equals the heat removed from the condenser minus the heat generated due to rotation.

The measurement of the heat due to rotation was determined at three different RPM's. Cooling water flow was established at a constant rate and electric power to the evaporator heater was secured. When steady state conditions were established, the temperature difference of the cooling water and the mass flow rate were recorded. The heat removed from the condenser was calculated using the mass flow rate and temperature difference across the condenser as described in Appendix B.

Evaporator wall temperature, wall saturation temperature, and heat flux were then calculated by the second method described in Appendix B. The specific data taken were enumerated under "Operating Procedure". All reduced data appear in Appendix E.

Data runs 1 thru 5 were taken at constant RPM with varying values of heat flux. Data taking began at 25 G's up to 400 G's. The liquid annulus thickness decreased from .4 inches at run 1 to .19 inches at run 5. Data runs 6 thru 11 were also taken at constant RPM and varying heat flux. In this series run 6 started at 400 G's and decreased to 25 G's

during run 11. The liquid annulus thickness decreased from .62 inches during run 6 to .38 inches during run 11. Data runs 12 thru 16 were taken at constant heat flux with varying values of RPM. Liquid annulus thickness decreased from .38 inches to .25 inches during this series of runs. Data run 17 was taken at a constant gravity level, 25 G's, and a constant heat flux of 80,000 BTU/hr ft^2. This run was taken to determine the effect of liquid annulus thickness of the heat transfer coefficient. Liquid annulus thickness started at .5 inches and decreased to .125 inches. Data run 18 was taken at 400 G's with varying values of heat flux. Liquid annulus thickness started at .63 inches and decreased to .56 inches. This run was taken to determine if there was any effect upon the data due to increasing the waiting time after each variable change to at least 15 minutes. This was well beyond the time that steady state appeared to have been established from the indicator values.

Visual observations of the state of the liquid in the evaporator were made during each data run. A stroboscope instrument was used to light the evaporator interior. At low gravity levels agitated nucleate boiling took place in the liquid annulus at all heat flux levels. The degree of turbulence increased as heat flux increased. At high gravity levels the nucleate boiling process increased very slowly as heat flux levels were increased. The degree of turbulence was much less at high gravity levels. Any effect of liquid

annulus thickness variation upon nucleate boiling was not readily apparent from visual observations.

IX. DISCUSSION OF RESULTS

Figure 4 shows the results of data runs 2 thru 5. RPM was held constant and heat flux was varied. Gravity levels started at 50 G's and progressed to 400 G's. Liquid annulus thickness was approximately .2 inches during this series. This figure shows that at low heat fluxes heat transfer is improved as gravity levels increase. There is no crossover region discernible, although the data appears to merge together at high heat fluxes.

Figure 5 shows the results of data runs 6 thru 9. RPM was again held constant and heat flux was varied. Liquid annulus thickness was approximately .5 inches. Data taking started at 400 G's and decreased to 50 G's. Again higher gravity levels show improved heat transfer rates at low values of heat flux. In this figure there is a definite crossover of the 100, 200, and 400 G curves. The data at 50 G's appears to be offset at superheats which are too high.

Figure 6 shows the results of data runs 11 thru 16. Liquid annulus thickness was approximately .38 inches during these runs. Heat flux was held constant and RPM was varied. There is a definite improvement in heat transfer with increasing gravity level, but no crossover region is evident.

Figure 7 shows the effect of liquid annulus change on the heat transfer coefficient. As the thickness of the annulus decreases, the heat transfer coefficient increases.

This agrees with the results of the investigation of MacKenzie [12] and the results of Ref. 13.

Figure 8 illustrates the effect of extending the waiting time at each data point from 5 - 7 minutes up to 15 minutes. This figure is a comparison between data runs 6 and 18. It appears that the longer the waiting time the more reliable the data. Even though the parameter indicators show that steady state has been established after approximately 5 minutes, waiting until at least 15 minutes results in a larger temperature difference and a higher heat flux. Thus it takes much longer than is readily apparent to reach steady state conditions.

Figure 9 is a comparison between data collected at 25 G's during these tests and data presented in Ref. 2 at 20 G's and in Ref. 8 at 25 G's. There is good correlation between the results of Ref. 2, but the data of Ref. 8 has higher values of superheat.

Figure 10 illustrates the data collected at 50 G's with that presented in Ref. 8 at the same gravity level. The 50 G data from Ref. 8 is offset in the direction of higher superheat. A possible explaination for this is different surface conditions and ageing effects between their test surface and the copper surface used here.

Figure 11 is a comparison between the 400 G data during this test and the 400 G data presented in Ref. 8. There is good correlation between both investigations.

V. CONCLUSIONS AND RECOMMENDATIONS

A. CONCLUSIONS

1. During nucleate pool boiling at low heat flux levels, there is a definite improvement in heat transfer with increasing gravity levels.
2. At higher heat flux levels some data shows a crossover trend while other data appear to just merge. No definite conclusion can be drawn from the available information.
3. Increasing the waiting time after any variable change beyond the apparent time of steady state enhances the reliability of the data.
4. Variations in the liquid annulus thickness cause changes in the heat transfer coefficient.

B. RECOMMENDATIONS

1. Increase the waiting time after any variable change to at least 15 minutes to increase the reliability of the data.
2. Operate with the machine closed to the atmosphere so that steaming is prevented and heat flux levels can be raised above those obtained in this investigation. This will necessitate a device for measuring the temperature or pressure in the evaporator vapor space.

3. Provide fins on the outside of the condenser to increase the heat transfer rate to the cooling water.
4. Increase the evaporator wall thickness so that larger temperature differences can be realized.
5. Install a permanent photographic installation so that the boiling phenomenon can be visually recorded.

APPENDIX A

CALIBRATION OF THERMOCOUPLES

The copper-constant thermocouples were calibrated using the Hewlett-Packard Data Acquisition System, 2010C, for millivolt readout. The following fixed point calibrations were made:

a. Ice point of water (32.0 °F)

b. Boiling point of water (212.0 °F at 14.696 psia)

c. Melting point of tin (449.4 °F)

d. Melting point of lead (621.1 °F)

Calibration of the ice point of water was accomplished by using a Thermos bottle filled with crushed ice and distilled water. Each thermocouple was inserted in this ice bath and three separate sets of data were recorded. The average value of these three data sets was used.

For boiling point of water, a large test tube was filled with distilled water, and a loose fitting cork with a hole in the center was inserted. Each thermocouple was inserted through the hole in the cork to approximately 1/2 inch above the water level when violent boiling had occurred. Four separate sets of data were taken and the average value used. An uncertainty for each thermocouple was also calculated using the highest and lowest reading. The largest value was ±.009 millivolts. The standard temperature was corrected for atmospheric pressure variation using the correction formula given in Ref. [7].

Calibration at the melting point of tin was accomplished by heating a pure tin sample in a large test tube. A small diameter glass tube with one end closed was inserted into the sample. Then the thermocouple to be calibrated was placed in the glass tube. A high range glass thermometer was also inserted in the sample. The temperature of the sample was then raised above the melting point and the heat withdrawn. The molten sample was allowed to cool until the freezing temperature was reached. Then for a discernible amount of time the temperature stabilized. At this point data was taken. This procedure was repeated six times inorder to insure accurate results. The average of the six data points was used and an uncertainty value was then calculated for each thermocouple. The largest uncertainty value was ±.004 millivolts.

The same physical setup was used to calibrate the thermocouples at the melting point of lead as was used for tin. As the lead was cooled in the molten state to its melting point, it did not stablize for any appreciable time. Therefore a tape printout was obtained using the minimum time interval possible. This data was then plotted on graph paper and the area of minimum slope was used as the calibration point. The average reading in this area of minimum slope was determined and uncertainty value again calculated. The largest uncertainty value was ±.1 millivolts.

Reference 14 recommends a third order equation of the form

$$E = at + bt^2 + ct^3$$

for interpolating thermocouple readings between 100 °C and approximately 300 °C. Using this equation and the calibration temperatures, the constants were determined using the IBM 360 computer for each thermocouple. Then using this result, a table of thermocouple readings versus degrees Centigrade and Fahrenheit was calculated for each thermocouple using the computer.

The results of the interpolating equation were plotted every 50 °C inorder to compare these values with the experimental data. At the three experimental points the uncertainty values were also plotted. The calculated results compared well with the experimental data.

APPENDIX B

DATA REDUCTION

A. CALCULATION OF EVAPORATOR WALL SATURATION PRESSURE

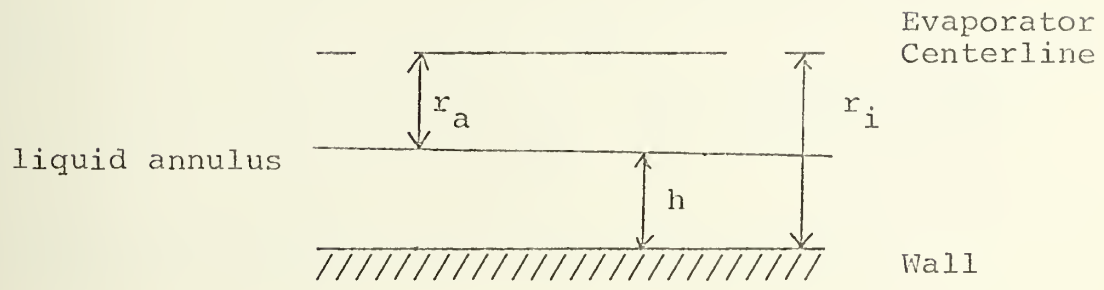

r_i = evaporator inner radius

r_a = distance from centerline to liquid annulus

h = liquid annulus thickness

Therefore

$$r_a = r_i - h$$

Squaring both sides of the equation

$$r_a^2 = r_i^2 - 2r_i h + h^2$$

The assumptions in this calculation were that solid body rotation takes place and that the density of the two phase mixture could be approximated by the density of water at 212 °F. This type of rotation of a fluid moving as a solid about an axis is called forced-vortex motion [15]. The pressure field varies with radial and axial position. Since the machine was maintained in the horizontal position there was no axial variation in pressure, and since rotation was at high RPM, earth's gravity was neglected. The radial component of the pressure becomes:

$$\frac{\partial P}{\partial r} = \frac{\rho_L w^2 r}{gc} \qquad (1)$$

where ρ_L = density of liquid at 212 °F, Lbm/ft^2

w = angular velocity of evaporator, rad/sec

r = radial position, ft

gc = conversion factor, 32.17 ft-Lbm/Lbf-sec^2

P = pressure, Lbf/ft^2

Integrating equation (1) from r_a to r_i yields:

$$\Delta P = \frac{\rho_L w^2}{2gc} (r_i^2 - r_a^2)$$

Substituting for r_a^2 yields:

$$\Delta P = \frac{\rho_L w^2}{2gc} h (2r_i - h)$$

or

$$P_{satw} = P_{atm} + \frac{\rho_L w^2}{2gc} h (2r_i - h)$$

where P_{satw} = pressure at wall, Lbf/ft^2

P_{atm} = pressure in vapor space, Lbf/ft^2

B. CALCULATION OF EVAPORATOR WALL SATURATION TEMPERATURE

The subroutine for the method of least squares on the IBM 360 computer was used to find an appropriate polynomial to simulate the water saturation pressure-temperature curve. The limits of 14.0 to 50.0 psia were used and a fourth order polynomial gave excellent correlation between actual data and a number of selected test points.

The polynomial used was as follows:

$$T_{satw} = 139.435 + 6.92642P_{satw} - .168663P_{satw}^2 + .0024795P_{satw}^3 - .0000148866P_{satw}^4$$

where

T_{satw} = saturation temperature at evaporator wall, °F.

C. CALCULATION OF TEMPERATURE PROFILE

The heat flow through the evaporator wall during steady state conditions can be reduced to a one dimensional problem if there is no axial or circumferential heat conduction. Under these assumptions the steady state conduction equation in cylindrical coordinates is

$$\frac{1}{r}\frac{d}{dr}\left(k(T)r\frac{dT}{dr}\right) = 0 \qquad (1)$$

where r = radial coordinate

T = temperature

$k(T)$ = thermal conductivity of copper.

Integrating equation (1) once gives

$$k(T)r\frac{dT}{dr} = \text{constant} = B_1$$

The thermal conductivity is assumed to vary linearly with temperature. Therefore,

$$k(T) = ko + m(T-To) \qquad (2)$$

Data on the conductivity of copper was obtained from Ref. 16 . In the temperature range of interest, 0 °F to 260 °F, the conductivity of copper is a linear function of temperature. This data was plotted and ko and m, the slope, were determined graphically.

$$ko = 231.77 \text{ BTU/hr-ft-°F}$$

$$m = -.02222 \text{ BTU/hr-ft-°F}^2$$

$$To = 0 \text{ °F}$$

Substituting equation (2) into (1) and then integrating again gives:

$$[ko + m\ (T/2-To)]T = B_1 + B_2 \ln r$$

The subroutine for the method of least squares on the IBM 360 computer was used to find the constants B_1 and B_2. Using these constants and value of the inner wall radius, T_{wall} was extrapolated.

D. CALCULATION OF HEAT FLUX, Q/A

From Fourier's Law:

$$Q = 2\pi L\ [k(t)r\ \frac{dT}{dr}]$$

or

$$Q = 2\pi L\ B_1$$

The inside area of the evaporator is

$$A = 2\pi r_i L$$

Then

$$\frac{Q}{A} = \frac{Q}{2\pi r_i L} = \frac{B_1}{r_i} \quad , \qquad \frac{BTU}{hr\ ft^2}$$

E. CALCULATION OF HEAT FLUX, Q/A, (SECOND METHOD)

The heat transfer rate out of the condenser is

$$Q_{out} = \dot{m}\ C_L(T_2 - T_1) \quad (\frac{BTU}{hr})$$

where $\dot{m}$ = coolant mass flow rate $(\frac{Lbm}{hr})$

C_L = coolant specific heat $(\frac{BTU}{Lbm-°F})$

T_1 = coolant inlet temperature (°F)

T_2 = coolant exit temperature (°F)

Q_{out} computed was then corrected for the heat loss due to evaporator rotation.

Then Q/A for the evaporator = $\frac{Q_{out}\ corrected}{Area\ of\ heated\ surface}$ =

$\frac{Q_{out}\ corrected}{2\pi r_i L}$.

F. CALCULATION OF EVAPORATOR WALL TEMPERATURE, T_{wall} (SECOND METHOD)

For steady state conditions, the heat flow equation is

$$Q = \frac{2\pi kL\ (T_c - T_{wall})}{\ln \frac{r_c}{r_i}} \qquad [17]$$

where T_c = average of the two center thermocouple reading, °F

r_c = radial distance to thermocouples, ft.

Then dividing by the inside area of the evaporator gives:

$$Q/A = \frac{k(T_c - T_{wall})}{r_i \ln \frac{r_c}{r_i}}$$

Solving for T_{wall} yields:

$$T_{wall} = T_c - \frac{r_i \left(\ln \frac{r_c}{r_i}\right) (Q/A)}{k}$$

The value of k was assumed constant at 226.7, BTU/hr-ft °F.

APPENDIX C

UNCERTAINTY ANALYSIS

In order to determine the reliability of the data collected and to determine the most probable error, an uncertainty analysis was performed utilizing the Kline and McClintock technique [19]. The analysis was performed on the data taken during run 1 at 1 KW.

A. UNCERTAINTY IN THE CALCULATION OF HEAT FLUX

$$Q/A = q'' = \frac{\dot{m}\ cp\ \Delta T}{A}$$

$$\frac{Wq''}{q''} = \sqrt{\left(\frac{W_{\dot{m}}}{\dot{m}}\right)^2 + \left(\frac{W_{cp}}{cp}\right)^2 + \left(\frac{W_{\Delta T}}{\Delta T}\right)^2 + \left(\frac{W_A}{A}\right)^2} \qquad (1)$$

W = uncertainty in subscripted quantity

$q'' = 10{,}045$ BTU/hr-ft^2

cp = 1.005 BTU/Lbm °F

A = .2386 ft^2

$\dot{m}$ = 30%

ΔT = 2.18 °F

$W_{\dot{m}} = \pm .5\%$

$W_{\Delta T} = \pm .1$

$W_{cp} = \pm .001$

$W_A = \pm .00001$

Substituting into equation (1) yields:

$$\frac{Wq''}{q''} = .0487 = 4.87\%$$

B. UNCERTAINTY IN THE CALCUALTION OF EVAPORATOR WALL TEMPERATURE

$$T_{wall} = T_c - \frac{r_i \ln \frac{r_c}{r_i} q''}{k}$$

$$W_{Tw} = \sqrt{(W_{Tc})^2 + [\frac{q''}{k} (\ln \frac{r_c}{r_i} - \frac{1}{r_i}) W_{ri}]^2 + (\frac{q''}{k} \frac{r_i}{r_c} W_{rc})^2 + (\frac{r_i \ln \frac{r_c}{r_i} q''}{k^2} W_k)^2 + (\frac{r_i \ln \frac{r_c}{r_i}}{k} W_{q''})^2} \quad (2)$$

$r_i = .130$ L ft

$k = 226.7$ BTU/hr-ft-°F

$W_{ri} = \pm .001$

$r_c = .1398$ ft

$W_{Tc} = \pm 2$

$W_k = \pm .1$

$q'' = 10{,}045$ BTU/hr-ft^2

$W_{rc} = \pm .001$

$W_{q''} = \pm .0487$

Substituting into equation (2) yields:

$$\frac{W_{Tw}}{T_w} = \frac{2.05}{225.7} = .0092 = .92\%$$

C. UNCERTAINTY IN THE CALCULATION OF WALL SATURATION PRESSURE

$$P_{satw} = P_{atm} + \frac{\rho w^2}{2g_c} h(2\, r_i - h)$$

$$W_{P_{satw}} = \sqrt{(W_{P_{atm}})^2 + (\frac{w^2 h}{2g_c}(2r_i - h)W_\rho)^2 + (\frac{\rho wh^2}{g_c}(2r_i - h)W_{w2})^2 + (\frac{\rho w^2}{2g_c^2} h(2r_i - h)Wg_c)^2 + (\frac{h\rho w^2}{g_c} W_{r_i})^2 (\frac{\rho w^2}{2g_c}(2r_i - 2h)W_h)^2} \qquad (3)$$

$r_i = .1302$ ft

$W = 78.5$ rad/sec

$Wg_c = \pm .001$

$h = .0338$ BTU/hr-ft^2-°F

$W_{P_{atm}} = \pm 1.0$

$W_{r_i} = \pm .001$

$g_c = 32.17$ ft/sec^2

$W_\rho = \pm .05$

$W_h = \pm .032$

$L = 60$ Lbm/ft^3

$W_{w2} = \pm .1$

Substituting into equation (3) yields:

$$\frac{W_{P_{satw}}}{P_{satw}} = \frac{3.36}{2158.12} = .0015 = .15\%$$

D. UNCERTAINTY IN THE CALCULATION OF WALL SATURATION TEMPERATURE

$$T_{satw} = 139.434 + 6.92642\ P_{satw} - .168663\ P_{satw}^{2} + .0024795\ P_{satw}^{3} - .0000148866\ P_{satw}^{4}$$

$$W_{T_{satw}} = \sqrt{\left(\frac{\partial T_{satw}}{\partial P_{satw}}\right)^{2} W_{P_{satw}}} \qquad (4)$$

Substituting into equation (4) yields:

$$\frac{W_{T_{satw}}}{T_{satw}} = \frac{3.35}{212.95} = .015 = 1.5\%$$

The largest uncertainty appears in the calculation of the heat flux. This is due to the error in the mass flow rate measurement and to the error in the coolant flow temperature difference measurement.

APPENDIX D

FIGURES

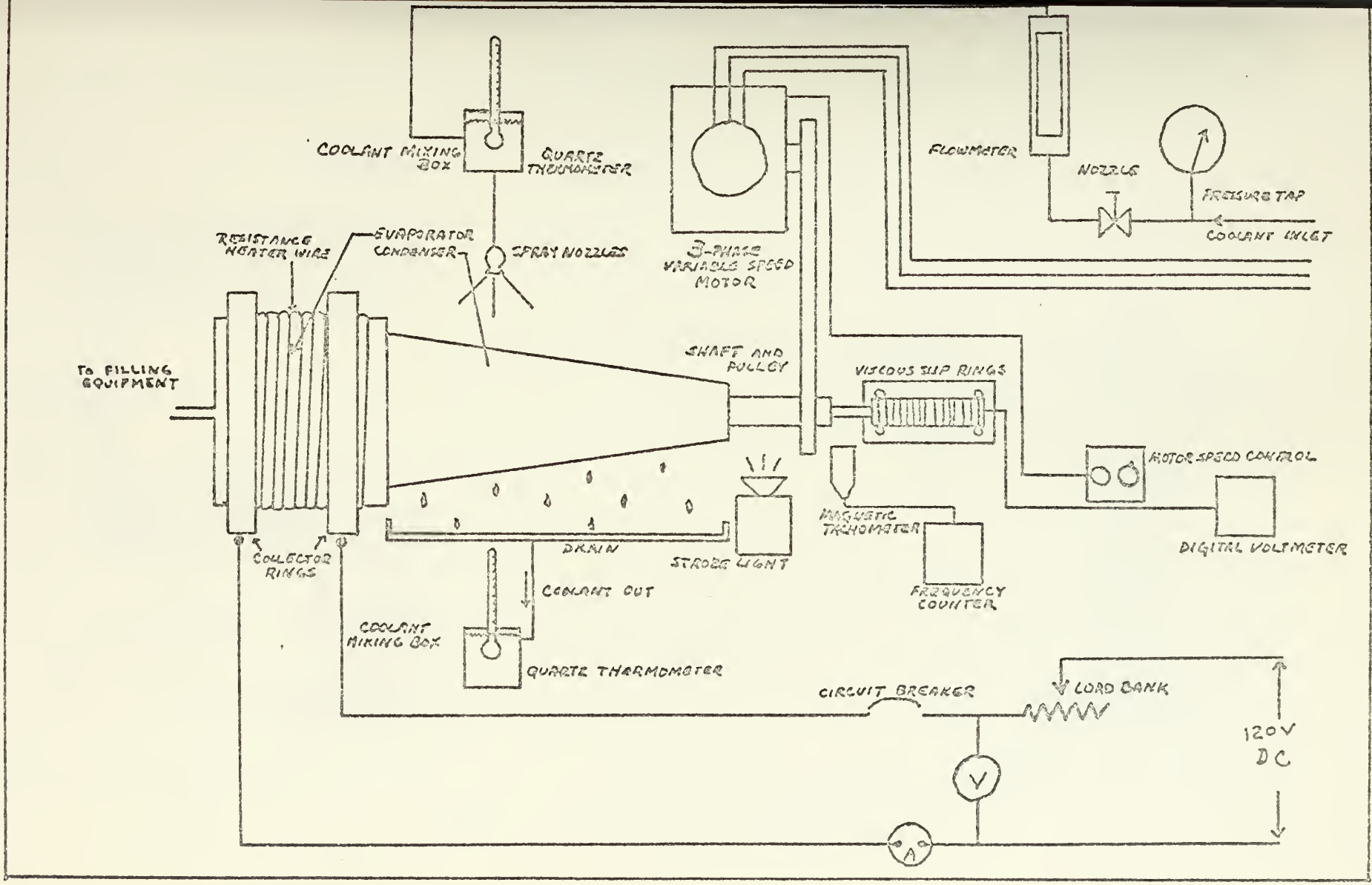
COOLANT MIXING BOX
QUARTZ THERMOMETER
FLOWMETER
NOZZLE
PRESSURE TAP
COOLANT INLET
3-PHASE VARIABLE SPEED MOTOR
RESISTANCE HEATER WIRE
EVAPORATOR CONDENSER
SPRAY NOZZLES
TO FILLING EQUIPMENT
SHAFT AND PULLEY
VISCOUS SLIP RINGS
MOTOR SPEED CONTROL
MAGNETIC TACHOMETER
DIGITAL VOLTMETER
COLLECTOR RINGS
DRAIN
STROBE LIGHT
FREQUENCY COUNTER
COOLANT OUT
COOLANT MIXING BOX
QUARTZ THERMOMETER
CIRCUIT BREAKER
LOAD BANK
120V DC
V
A

FIGURE 1.

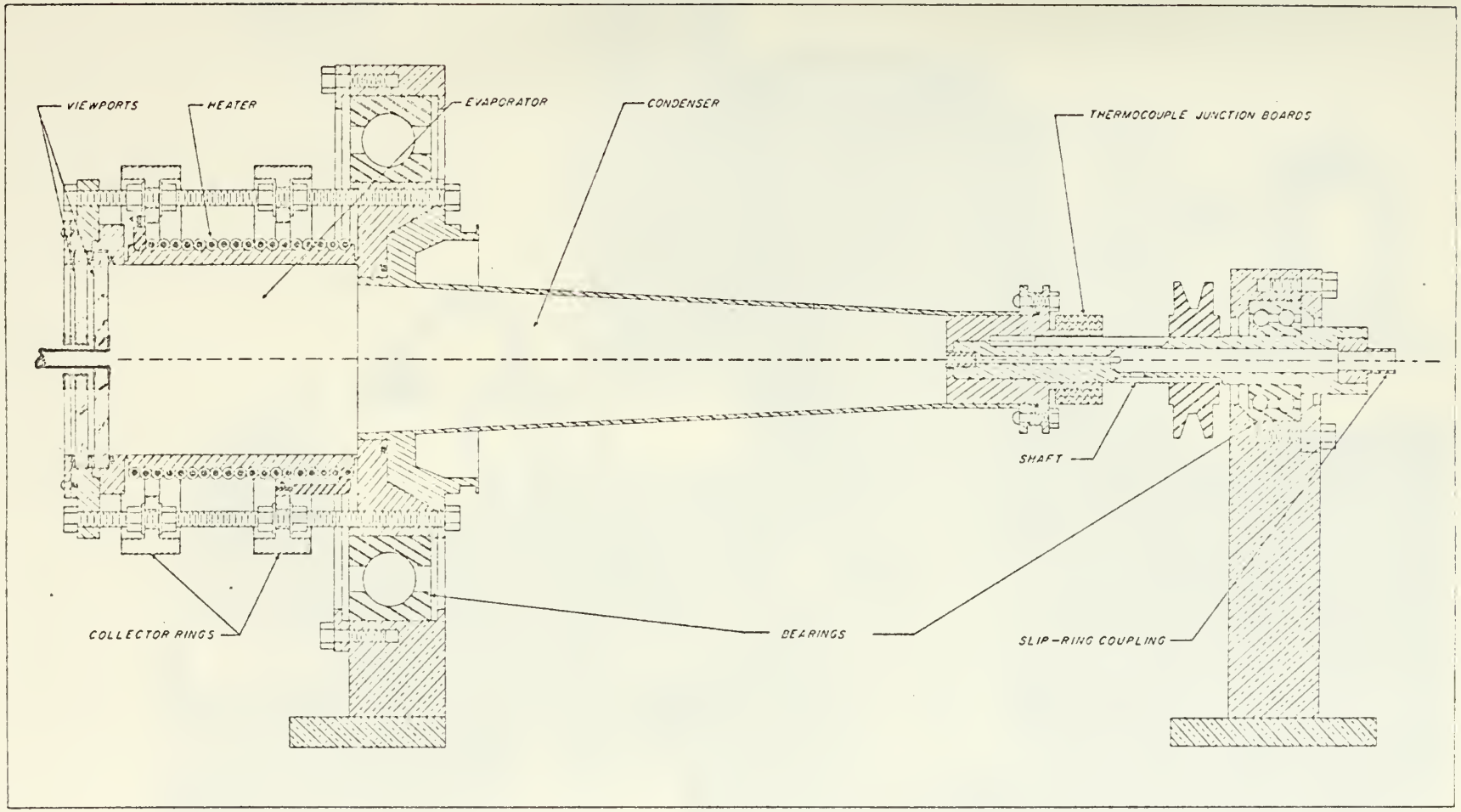

FIGURE 2. CROSS SECTION OF ROTATING HEAT PIPE

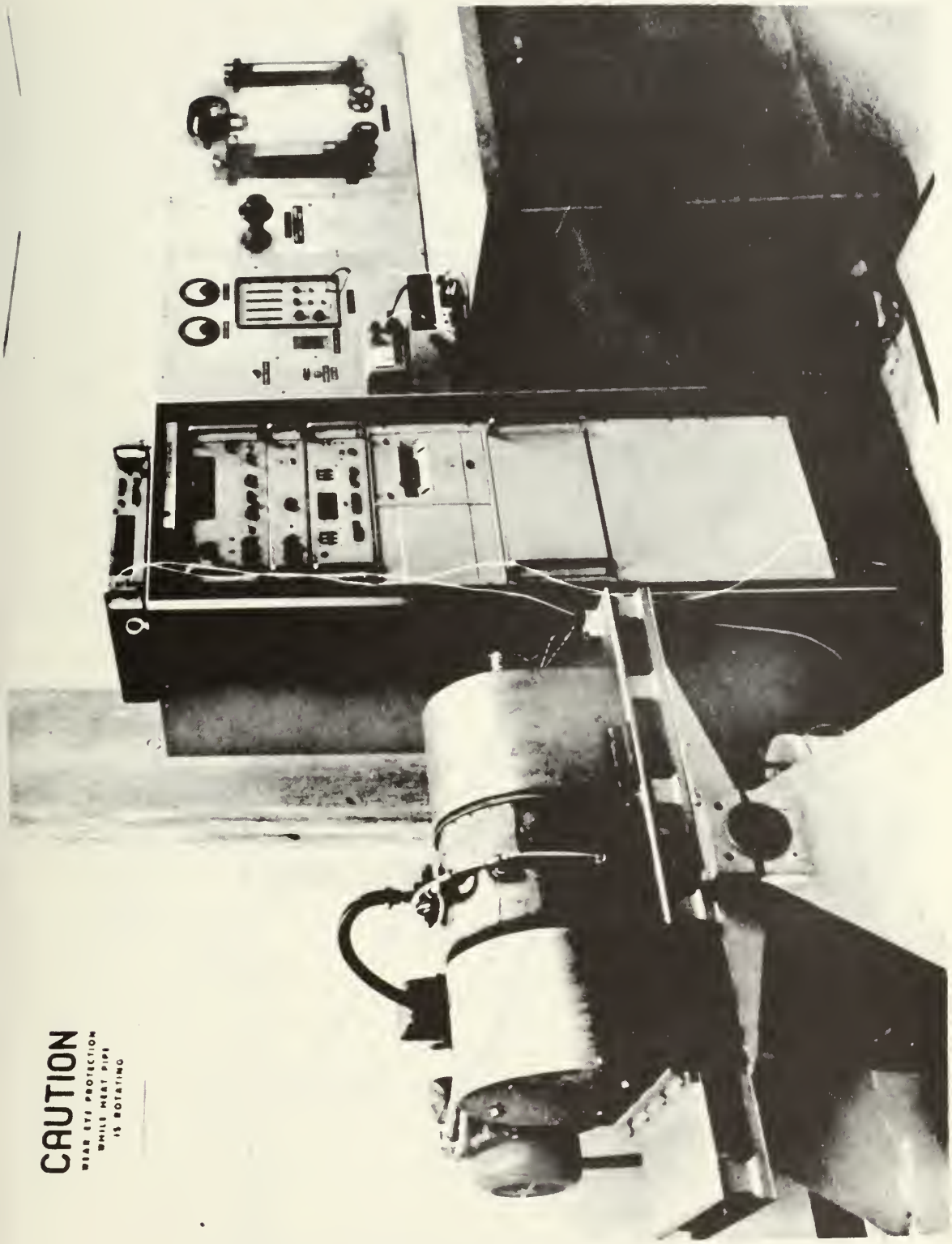

FIGURE 3.

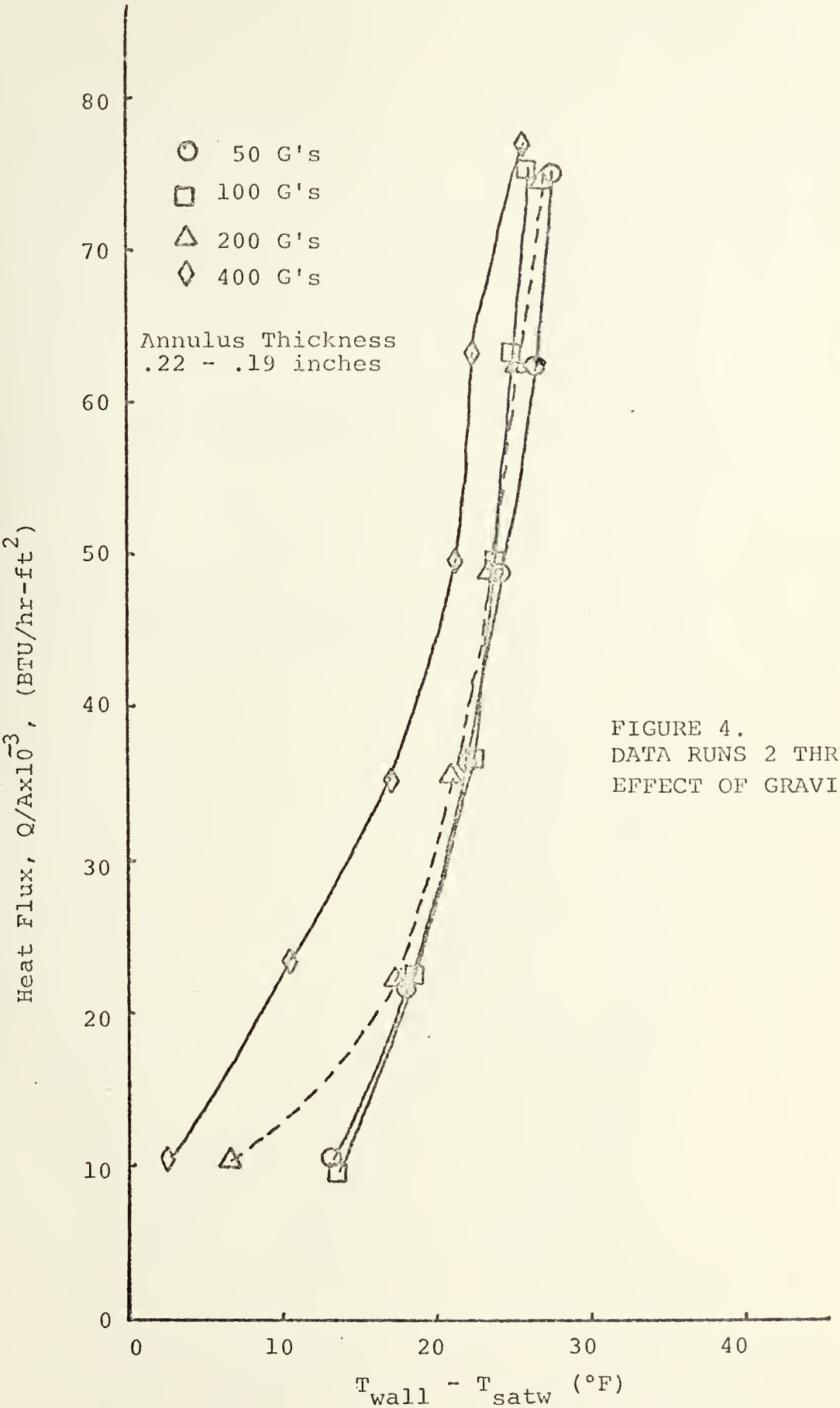

FIGURE 4.
DATA RUNS 2 THRU 5
EFFECT OF GRAVITY

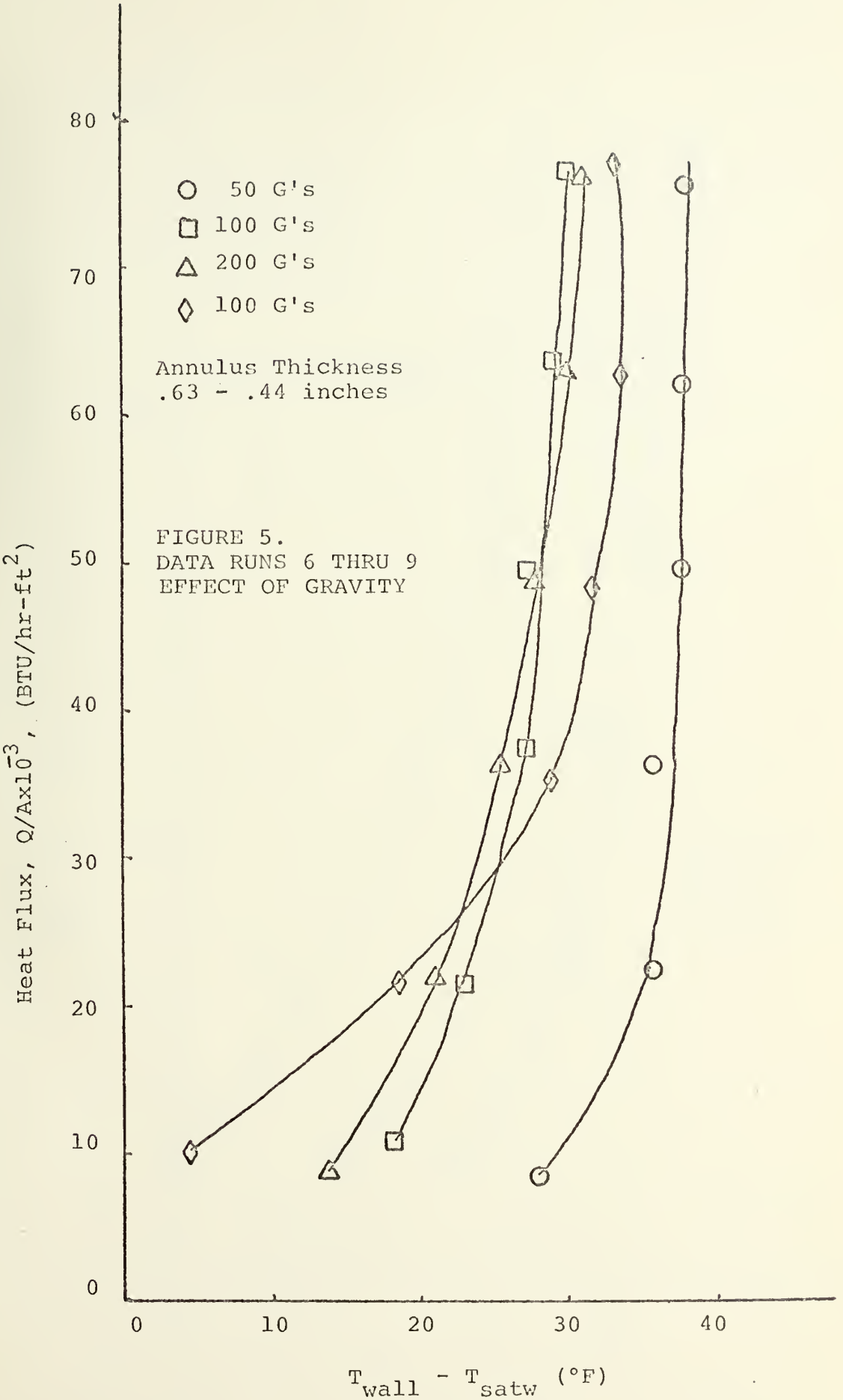

FIGURE 5.
DATA RUNS 6 THRU 9
EFFECT OF GRAVITY

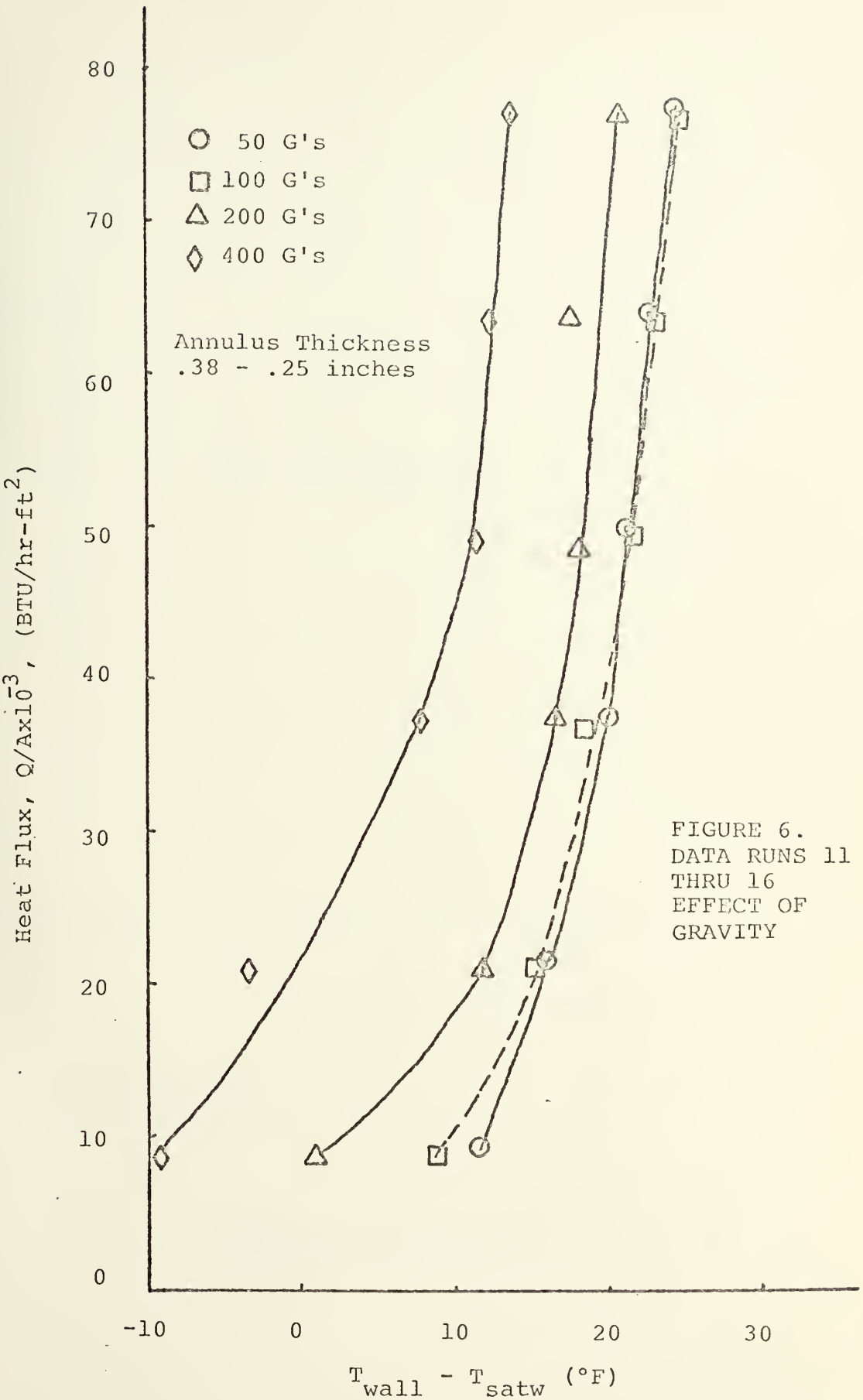

FIGURE 6.
DATA RUNS 11
THRU 16
EFFECT OF
GRAVITY

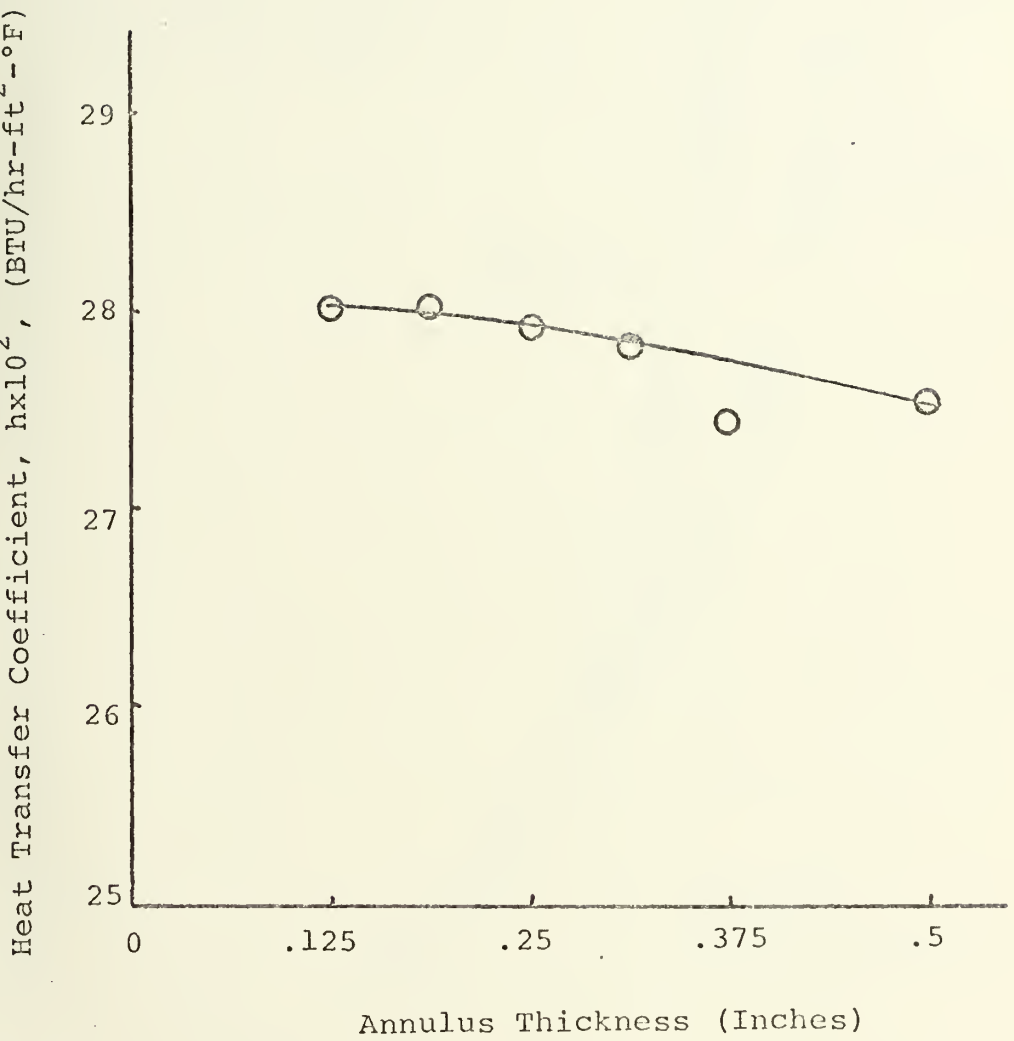

Gravity Level, 25 G's
Heat Flux, 80,000 BTU/hr-ft^2

FIGURE 7. EFFECT OF ANNULUS THICKNESS ON HEAT TRANSFER COEFFICIENT

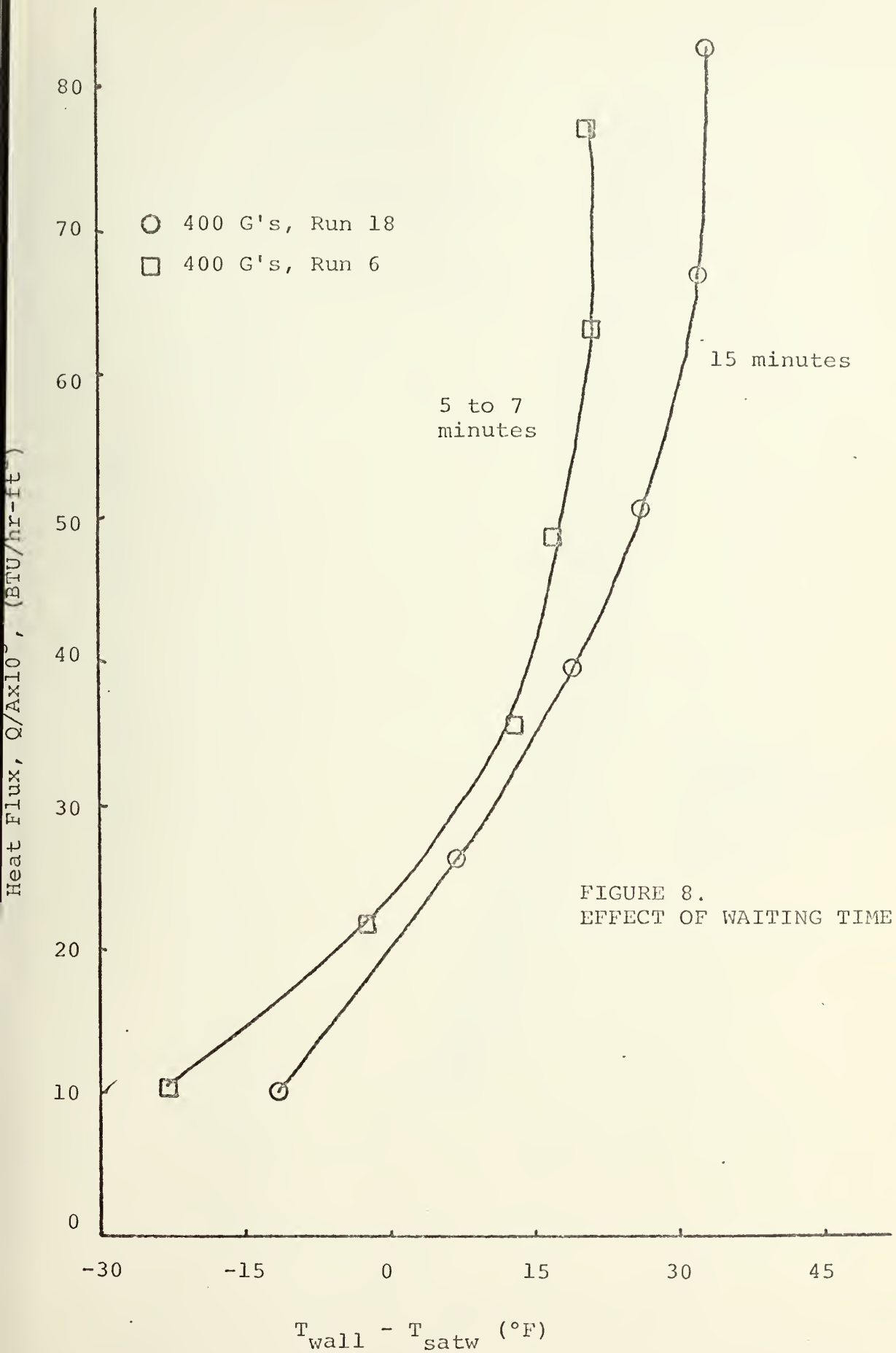

FIGURE 8.
EFFECT OF WAITING TIME

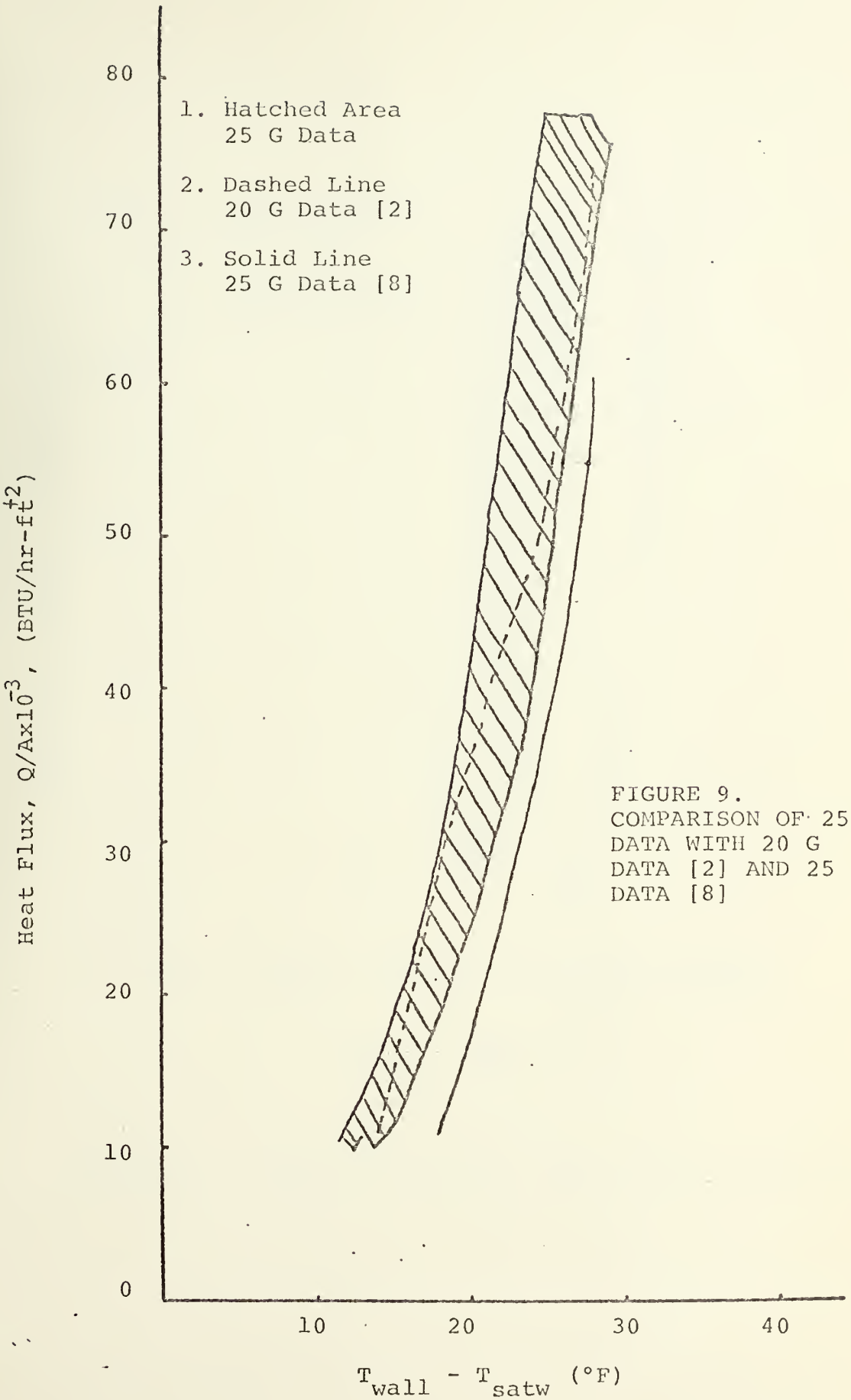

FIGURE 9.
COMPARISON OF 25 G DATA WITH 20 G DATA [2] AND 25 G DATA [8]

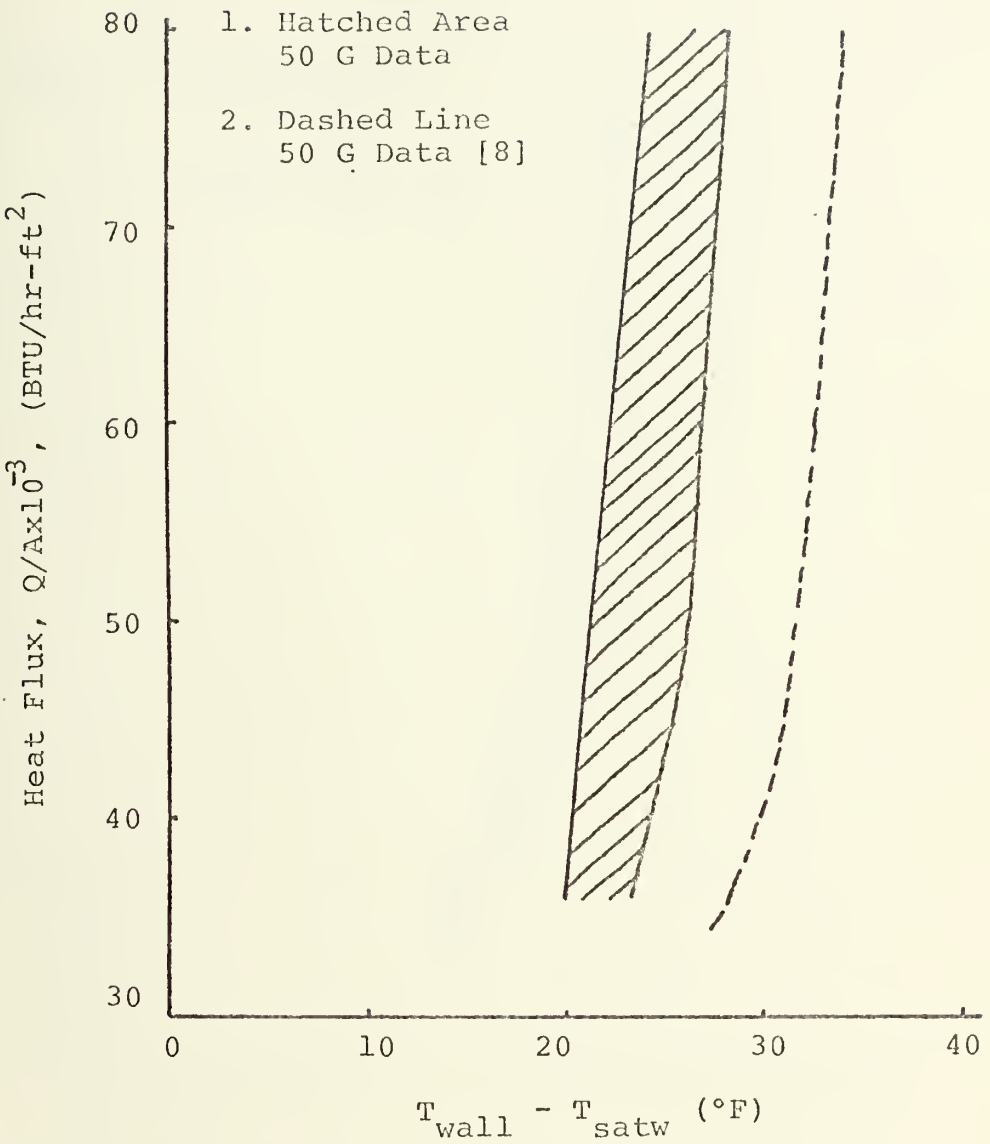

FIGURE 10. COMPARISION OF 50 G DATA AND 50 G DATA [8]

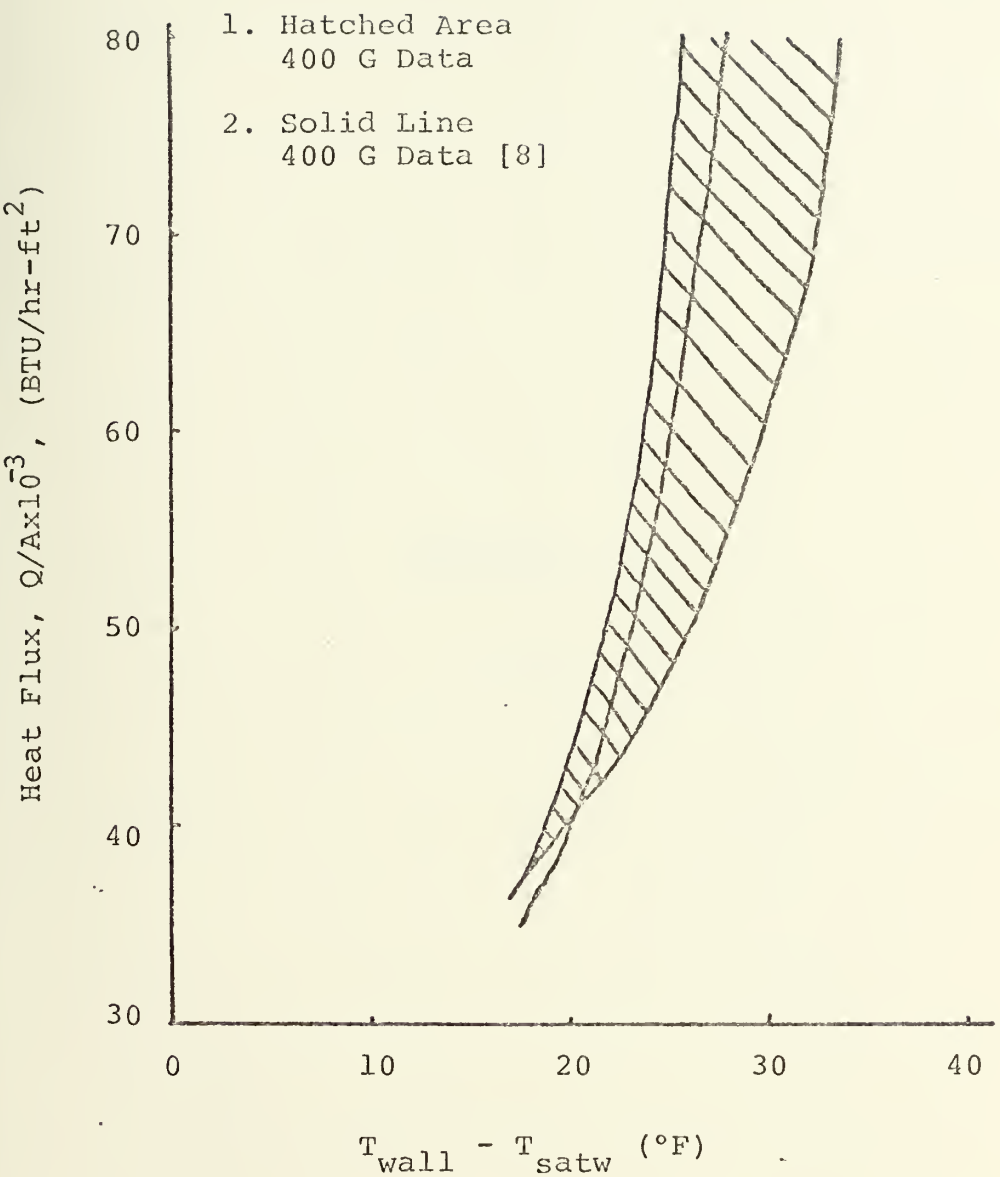

FIGURE 11. COMPARISON OF 400 G DATA AND 400 G DATA [8]

APPENDIX E

DATA

Run 1, P_{atm} 14.681, T_{satv} 211.95

RPM	G's	Annulus Thick-ness	P_{satw}	T_{satw}	T_{wall}	T_c	ΔT	$Q/Ax10^{-3}$	$hx10^{-2}$	$T_{wall} - T_{satw}$
750	25	.40625	14.987	212.95	225.7	226.1	2.18	10.045	7.89	12.74
750	25	.40625	14.987	212.95	231.9	233.0	5.35	24.655	12.95	19.04
750	25	.40625	14.987	212.95	233.6	235.1	8.06	37.190	18.03	20.62
750	25	.40625	14.987	212.95	235.7	237.8	11.32	52.215	22.99	22.71
750	25	.40625	14.987	212.95	237.3	240.0	14.06	64.833	26.82	24.39
750	25	.40625	14.987	212.95	237.9	241.0	16.20	74.712	29.92	24.99

Run 2, P_{atm} 14.681, T_{satv} 211.95

RPM	G's	Annulus Thick-ness	P_{satw}	T_{satw}	T_{wall}	T_c	ΔT	$Q/Ax10^{-3}$	$hx10^{-2}$	$T_{wall} - T_{satw}$
1062	50	.21875	15.034	213.11	226.9	227.3	2.16	9.962	7.23	13.78
1062	50	.21875	15.034	213.11	231.9	232.8	4.93	22.746	12.13	18.76
1062	50	.21875	15.034	213.11	235.7	237.2	7.90	36.443	16.13	22.60
1062	50	.21875	15.034	213.11	237.1	239.1	10.82	49.891	20.83	23.95
1062	50	.21875	15.034	213.11	238.2	240.8	13.64	62.924	25.06	25.11
1062	50	.21875	15.034	213.11	239.2	242.3	16.31	75.210	28.81	26.11

Run 3, P_{atm} 14.681, T_{satv} 211.95

RPM	G's	Annulus Thick-ness	P_{satw}	T_{satw}	T_{wall}	T_c	ΔT	$Q/Ax10^{-3}$	$hx10^{-2}$	$T_{wall} - T_{satW}$
1502	100	.1875	15.293	213.97	227.2	227.6	2.25	10.376	7.85	13.21
1502	100	.1875	15.293	213.97	232.5	233.4	4.70	21.664	11.69	18.54
1502	100	.1875	15.293	213.97	236.2	237.7	7.87	36.277	16.30	22.25
1502	100	.1875	15.293	213.97	238.6	240.6	10.64	49.061	19.93	24.62
1502	100	.1875	15.293	213.97	240.5	243.0	13.52	62.343	23.54	26.48
1502	100	.1875	15.293	213.97	241.5	244.6	16.25	74.961	27.20	27.56

Run 4, P_{atm} 14.681, T_{satv} 211.95

RPM	G's	Annulus Thick-ness	P_{satw}	T_{satw}	T_{wall}	T_c	ΔT	$Q/Ax10^{-3}$	$hx10^{-2}$	$T_{wall}-T_{satw}$
2124	200	.1875	15.905	215.96	222.7	223.1	2.23	10.294	15.32	6.72
2124	200	.1875	15.905	215.96	233.6	234.5	4.82	22.248	12.62	17.63
2124	200	.1875	15.905	215.96	237.4	238.9	7.78	35.862	16.70	21.47
2124	200	.1875	15.905	215.96	239.8	241.8	10.64	49.061	20.59	23.83
2124	200	.1875	15.905	215.96	241.5	244.1	13.63	62.841	24.58	25.57
2124	200	.1875	15.905	215.96	242.9	246.0	16.22	74.795	27.72	26.98

Run 5, P_{atm} 14.681, T_{satv} 211.95

RPM	G's	Annulus Thick-ness	P_{satw}	T_{satw}	T_{wall}	T_c	ΔT	$Q/Ax10^{-3}$	$hx10^{-2}$	$T_{wall} - T_{satW}$
3003	400	.1875	17.128	219.77	222.6	223.0	2.34	10.792	38.67	2.79
3003	400	.1875	17.128	219.77	230.4	231.4	5.09	23.493	22.02	10.67
3003	400	.1875	17.128	219.77	237.0	238.5	7.87	36.277	21.03	17.25
3003	400	.1875	17.128	219.77	241.3	243.3	10.84	49.974	23.25	21.49
3003	400	.1875	17.128	219.77	242.1	244.7	13.73	63.339	28.35	22.34
3003	400	.1875	17.128	219.77	245.3	248.5	16.70	77.036	30.12	25.58

Run 6, P_{atm} 14.774, T_{satv} 212.26

RPM	G's	Annulus Thick-ness	P_{satw}	T_{satw}	T_{wall}	T_c	ΔT	$Q/Ax10^{-3}$	$hx10^{-2}$	$T_{wall} - T_{satW}$
3003	400	.625	21.72	232.39	208.0	209.0	2.23	10.293	-4.48	-23.0
3003	400	.625	21.72	232.39	230.4	231.3	4.73	21.832	-108.08	-2.02
3003	400	.625	21.72	232.39	246.1	247.6	7.74	35.696	26.09	13.68
3003	400	.625	21.72	232.39	250.1	252.2	10.55	48.646	27.45	17.72
3003	400	.625	21.72	232.39	253.7	256.4	13.68	63.090	29.62	21.30
3003	400	.625	21.72	232.39	252.7	256.0	16.81	77.534	38.23	20.28

Run 6 (Continued)

RPM	G's	Annulus Thick-ness	P_{satw}	T_{satw}	T_{wall}	T_c	ΔT	$Q/Ax10^{-3}$	$hx10^{-2}$	$T_{wall} - T_{satw}$
3003	400	.625	21.72	232.39	250.2	253.0	14.36	66.244	37.28	17.77
3003	400	.625	21.72	232.39	244.8	247.0	10.94	50.472	40.54	12.45
3003	400	.625	21.72	232.39	238.1	239.7	8.17	37.688	66.24	5.69
3003	400	.625	21.72	232.39	227.7	228.6	5.33	24.572	-51.19	-4.8
3003	400	.625	21.72	232.39	217.2	217.7	2.38	10.958	-7.23	-15.16

Run 7, P_{atm} 14.725, T_{satv} 212.10

RPM	G's	Annulus Thick-ness	P_{satw}	T_{satw}	T_{wall}	T_c	ΔT	$Q/Ax10^{-3}$	$hx10^{-2}$	$T_{wall} - T_{satw}$
2124	200	.5	17.64	221.30	211.9	212.3	1.93	8.882	-9.46	-9.39
2124	200	.5	17.64	221.30	223.0	224.0	4.79	22.082	126.9	1.75
2124	200	.5	17.64	221.30	230.1	231.7	7.90	36.443	41.27	8.83
2124	200	.5	17.64	221.30	233.9	236.0	10.64	49.061	38.97	12.59
2124	200	.5	17.64	221.30	236.7	239.4	13.70	63.173	41.08	15.38
2124	200	.5	17.64	221.30	238.5	241.8	16.58	76.455	44.40	17.22

Run 8, P_{atm} 14.725, T_{satv} 212.10

RPM	G's	Annulus Thick-ness	P_{satw}	T_{satw}	T_{wall}	T_c	ΔT	$Q/Ax10^{-3}$	$hx10^{-2}$	$T_{wall}-T_{satw}$
1502	100	.5	16.184	216.84	214.1	214.6	2.39	11.041	-40.59	-2.72
1502	100	.5	16.184	216.84	221.4	222.3	4.70	21.666	47.82	4.53
1502	100	.5	16.184	216.84	227.9	229.5	8.10	37.356	33.78	11.06
1502	100	.5	16.184	216.84	228.4	230.6	10.73	49.476	42.51	11.64
1502	100	.5	16.184	216.84	231.1	233.8	13.82	63.754	44.80	14.23
1502	100	.5	16.184	216.84	232.3	235.6	16.61	76.621	49.53	15.47

Run 9, P_{atm} 14.647, T_{satv} 211.83

RPM	G's	Annulus Thick-ness	P_{satw}	T_{satw}	T_{wall}	T_c	ΔT	$Q/Ax10^{-3}$	$hx10^{-2}$	$T_{wall}-T_{satw}$
1062	50	.4375	15.30	213.99	225.9	226.3	1.89	8.716	7.29	11.95
1062	50	.4375	15.30	213.99	237.8	238.7	4.90	22.580	9.50	23.78
1062	50	.4375	15.30	213.99	237.2	238.7	7.85	36.194	15.58	23.23
1062	50	.4375	15.30	213.99	239.7	241.7	10.75	49.559	19.30	25.68
1062	50	.4375	15.30	213.99	240.9	243.5	13.46	62.094	23.03	26.96
1062	50	.4375	15.30	213.99	241.9	245.0	16.42	75.708	27.13	27.91

Run 10, P_{atm} 14.647, T_{satv} 211.83

RPM	G's	Annulus Thick-ness	P_{satw}	T_{satw}	T_{wall}	T_c	ΔT	$Q/Ax10^{-3}$	$hx10^{-2}$	$T_{wall} - T_{satw}$
750	25	14.953	212.83	227.8	227.8	228.3	2.48	11.456	7.64	14.99
750	25	14.953	212.83	227.8	232.1	233.1	5.06	23.327	12.08	19.31
750	25	14.953	212.83	227.8	237.0	238.6	8.06	37.190	15.34	24.24
750	25	14.953	212.83	227.8	238.3	240.3	10.73	49.476	19.46	25.43
750	25	14.953	212.83	227.8	240.4	243.0	13.86	63.920	23.21	27.54
750	25	14.953	212.83	227.8	241.9	245.0	16.51	76.123	26.21	29.04

Run 11, P_{atm} 14.789, T_{satv} 212.32

RPM	G's	Annulus Thick-ness	P_{satw}	T_{satw}	T_{wall}	T_c	ΔT	$Q/Ax10^{-3}$	$hx10^{-2}$	$T_{wall}-T_{satw}$
750	25	.375	15.075	213.25	224.9	225.4	2.36	10.875	9.29	11.71
1062	50	.375	15.36	214.19	225.5	225.9	2.00	9.214	8.13	11.33
1502	100	.375	15.94	216.05	224.8	225.2	1.89	8.716	9.92	8.79
2124	200	.375	17.08	219.63	221.2	220.8	1.91	8.799	72.72	1.21
3003	400	.375	19.37	226.24	217.34	217.7	1.93	8.882	-9.98	-8.90

Run 12, P_{atm} 14.789, T_{satv} 212.32

RPM	G's	Annulus Thick-ness	P_{satw}	T_{satw}	T_{wall}	T_c	ΔT	$Q/Ax10^{-3}$	$hx10^{-2}$	$T_{wall}-T_{satw}$
750	25	.375	15.07	213.25	230.1	231.1	5.11	23.576	13.96	16.89
1062	50	.375	15.36	214.19	230.2	231.1	4.75	21.915	13.69	16.01
1502	100	.375	15.94	216.05	231.5	232.4	4.61	21.251	13.73	15.48
2124	200	.375	17.08	219.63	231.7	232.6	4.59	21.168	17.48	12.12
3003	400	.375	19.37	226.24	222.8	223.7	4.59	21.168	-6.21	-3.41

Run 13, P_{atm} 14.789, T_{satv} 212.32

RPM	G's	Annulus Thick-ness	P_{satw}	T_{satw}	T_{wall}	T_c	ΔT	$Q/Ax10^{-3}$	$hx10^{-2}$	T_{wall} - T_{satW}
750	25	.375	15.07	213.25	233.2	234.8	8.53	39.348	19.73	19.94
1062	50	.375	15.36	214.19	234.4	235.9	8.14	37.522	18.60	20.17
1502	100	.375	15.94	216.05	234.9	235.9	8.01	36.941	20.15	18.33
2124	200	.375	17.08	219.63	236.4	237.9	8.21	37.854	22.64	16.72
3003	400	.375	19.37	226.24	235.8	235.8	8.17	37.688	47.05	8.01

Run 14, P_{atm} 14.789, T_{satv} 212.32

RPM	G's	Annulus Thick-ness	P_{satw}	T_{satw}	T_{wall}	T_c	ΔT	$Q/Ax10^{-3}$	$hx10^{-2}$	$T_{wall} - T_{satw}$
750	25	.375	15.07	213.25	234.6	236.7	11.27	51.966	24.63	21.33
1062	50	.375	15.36	214.20	235.6	237.6	10.84	49.974	23.40	21.36
1502	100	.375	15.94	216.05	237.2	239.2	10.76	49.642	23.52	21.11
2124	200	.375	17.08	219.63	238.0	240.0	10.58	48.812	26.56	18.38
3003	400	.375	19.37	226.24	237.7	239.7	10.64	49.061	42.89	11.44

Run 15, P_{atm} 14.789, T_{satv} 212.32

RPM	G's	Annulus Thick-ness	P_{satw}	T_{satw}	T_{wall}	T_c	ΔT	$Q/Ax10^{-3}$	$hx10^{-2}$	$T_{wall} - T_{satw}$
750	25	.3438	15.05	213.18	236.7	238.4	14.36	66.245	29.43	22.51
1062	50	.3438	15.32	214.06	236.8	239.4	13.95	64.335	28.33	22.71
1502	100	.3438	15.85	215.78	238.6	241.2	13.81	63.671	27.91	22.81
2124	200	.3438	16.91	219.12	263.8	239.4	13.86	63.920	36.17	17.67
3003	400	.3438	19.04	225.32	237.7	240.3	13.86	63.920	51.72	12.36

Run 16, P_{atm} 14.789, T_{satv} 212.32

RPM	G's	Annulus Thick-ness	P_{satw}	T_{satw}	T_{wall}	T_c	ΔT	$Q/Ax10^{-3}$	$hx10^{-2}$	$T_{wall}-T_{satw}$
750	25	.25	14.99	212.96	238.2	241.4	16.81	77.534	30.68	25.27
1062	50	.25	15.19	213.62	237.8	241.0	16.76	77.285	31.92	24.21
1502	100	.25	15.59	214.93	239.0	242.2	16.78	77.368	32.11	24.10
2124	200	.25	16.39	217.48	238.4	241.6	16.79	77.451	36.97	20.95
3003	400	.25	17.98	222.31	236.0	239.2	16.74	77.202	56.23	13.73

Run 17, P_{atm} 14.789, T_{satv} 212.32

RPM	G's	Annulus Thick-ness	P_{satw}	T_{satw}	T_{wall}	T_c	ΔT	$Q/Ax10^{-3}$	$hx10^{-2}$	$T_{wall}-T_{satw}$
750	25	.5	15.02	213.06	242.0	245.3	17.30	79.776	27.54	28.97
750	25	.375	14.94	212.80	241.9	245.2	17.33	79.942	27.45	29.12
750	25	.3125	14.90	212.66	241.6	244.9	17.46	80.523	27.82	28.94
750	25	.250	14.86	212.51	241.6	244.9	17.60	81.187	27.94	29.06
750	25	.1875	14.81	212.35	241.5	244.8	17.71	81.685	28.07	29.10
750	25	.125	14.76	212.19	241.5	244.9	17.82	82.183	28.01	29.34

Run 18, P_{atm} 14.557, T_{satv} 211.51

RPM	G's	Annulus Thick-ness	P_{satw}	T_{satw}	T_{wall}	T_c	ΔT	$Q/Ax10^{-3}$	$hx10^{-2}$	$T_{wall} - T_{satw}$
3003	400	.625	21.50	231.85	220.5	220.9	2.21	10.211	-8.98	-11.37
3003	400	.625	21.50	231.85	238.7	239.8	5.67	26.150	38.01	6.88
3003	400	.625	21.50	231.85	250.9	252.6	8.64	39.846	20.84	19.12
3003	400	.625	21.50	231.85	258.2	260.3	10.98	50.638	19.20	26.38
3003	400	.5625	20.96	230.48	262.6	265.3	14.51	66.909	20.86	32.08
3003	400	.5625		230.48	263.6	267.0	18.41	83.677	25.29	33.09

BIBLIOGRAPHY

1. Costello, C.P. and Tuthill, M.E., "Effects of Acceleration on Nucleate Pool Boiling," Chemical Engineering Progress Symposium Series, v. 57, No. 32, p. 189-196, 1961.

2. Merte, H. and Clark, J.A., "Pool Boiling in an Accelerating System," Journal of Heat Transfer, v. 83, series C, No. 3, p. 233-242, 1961.

3. Holman, J.P., Heat Transfer, 2d ed., p. 198, McGraw-Hill, 1968.

4. Adelberg, M., "Gravitational Effect Upon Nucleate Boiling Heat Transfer," Advances in the Astronautical Sciences, American Astronautical Society, v. 14, 1963.

5. Adelberg, M., Heat Transfer in Pool Nucleate Boiling, Technical Note 169.1-MA-11.1-3-67, 13 March 1967.

6. Graham, R.W. and Hendricks, R.C., "The Study of the Effect of Multi-G Acceleration on Nucleate Boiling Ebullition," NASA Technical Note D-1196, 1963.

7. Gray, V.H., Marto, P.J. and Joslyn, A.W., "Boiling Heat-Transfer Coefficients, Interface Behavior, and Vapor Quality in Rotating Boiler Operating to 475 G's," NASA Technical Note D-4136, March 1968.

8. Marto, P.J. and Gray, V.H., "Effects of High Accelerations and Heat Fluxes on Nucleate Boiling of Water in an Axisymmetric Rotating Boiler," NASA Technical Note D-6307, May 1971.

9. Judd, R.L. and Merte, H. Jr., "Evaluation of Nucleate Boiling Heat Flux Predictions at Varying Levels of Subcooling and Acceleration," Int. Journal of Heat and Mass Transfer, v. 15, p. 1075-1096, 1972.

10. Woodard, J.S., The Operation of Rotating Non-Capillary Heat Pipes, M.S. Thesis, Naval Postgraduate School, Monterey, California, March 1972.

11. Schafer, C.E., Augmenting the Heat Transfer Characteristics of the Rotating Two-Phase Thermosyphon, Engineer's Thesis, Naval Postgraduate School, Monterey, California, December 1972.

12. MacKenzie, D.K., Vaporization of Thin Liquid Films, M.S. Thesis, Naval Postgraduate School, Monterey, California, December 1972.

13. Nishikawa, K., Hisao, K., Yamasaki, K., and Tanaka, K., "Nucleate Boiling at Low Liquid Levels," Bulletin of JSME, v. 10, no. 38, p. 328-338, 1967.

14. Roeser, W.F. and Lonberger, S.T., "Methods of Testing Thermocouples and Thermocouple Material," National Bureau of Standards Circular 590, 6 February 1958.

15. Streeter, V.L., Fluid Mechanics, p. 74, McGraw-Hill, 1971.

16. Touloukian, Y.S., Thermophysical Properties of Matter, v. 1, p. 68-81, IFI/Plenum, 1972.

17. Holman, J.P., Heat Transfer, 2d ed., p. 22, McGraw-Hill, 1968.

18. Eckert, E.R.G. and Drake, R.M., Jr., Analysis of Heat and Mass Transfer, p. 70-71, McGraw-Hill, 1972.

19. Holman, J.P., Experimental Methods for Engineers, p. 36-40, McGraw-Hill, 1966.

INITIAL DISTRIBUTION LIST

		No. Copies
1.	Library, Code 0212 Naval Postgraduate School Monterey, California 93940	2
2.	Assoc. Professor P.J. Marto, Code 59 Department of Mechanical Engineering Naval Postgraduate School Monterey, California 93940	1
3.	LCDR Gibson P. Smith, USN 529 Castle Drive Moses Lake, Washington 98837	1
4.	Department of Mechanical Engineering Naval Postgraduate School Monterey, California 93940	1

Security Classification

DOCUMENT CONTROL DATA - R & D

(Security classification of title, body of abstract and indexing annotation must be entered when the overall report is classified)

ORIGINATING ACTIVITY (Corporate author)

Naval Postgraduate School
Monterey, California 93940

2a. REPORT SECURITY CLASSIFICATION

Unclassified

2b. GROUP

REPORT TITLE

The Effect of Gravity on Nucleate Pool Boiling of Water

DESCRIPTIVE NOTES (Type of report and, inclusive dates)

Master's Thesis; December 1972

AUTHOR(S) (First name, middle initial, last name)

Gibson Peter Smith

REPORT DATE	7a. TOTAL NO. OF PAGES	7b. NO. OF REFS
December 1972	75	19

CONTRACT OR GRANT NO.

PROJECT NO.

9a. ORIGINATOR'S REPORT NUMBER(S)

9b. OTHER REPORT NO(S) (Any other numbers that may be assigned this report)

DISTRIBUTION STATEMENT

Approved for public release; distribution unlimited.

SUPPLEMENTARY NOTES

12. SPONSORING MILITARY ACTIVITY

Naval Postgraduate School
Monterey, California 93940

ABSTRACT

The effect of gravity levels up to 400 times the local gravity value (a/g) was experimentally investigated in a copper, rotating, cylindrical boiler. Heat flux levels up to 80,000 BTU/hr-ft^2 were reached.

Observed improvement in heat transfer at low heat flux values with increasing gravity levels confirmed the results of previous investigations. At high heat flux values, a consistent trend was not observed. With increasing gravity levels, some data indicated a decrease in heat transfer while other data indicated an increase in heat transfer. Changes in heat transfer with variation of the liquid annulus thickness was noted.

DD FORM 1 NOV 68 1473 (PAGE 1)

S/N 0101-807-6811

Security Classification

A-31408

Security Classification

DOCUMENT CONTROL DATA - R & D

(Security classification of title, body of abstract and indexing annotation must be entered when the overall report is classified)

ORIGINATING ACTIVITY (Corporate author)

Naval Postgraduate School
Monterey, California 93940

2a. REPORT SECURITY CLASSIFICATION

Unclassified

2b. GROUP

REPORT TITLE

The Effect of Gravity on Nucleate Pool Boiling of Water

DESCRIPTIVE NOTES (Type of report and inclusive dates)

Master's Thesis; December 1972

AUTHOR(S) (First name, middle initial, last name)

Gibson Peter Smith

REPORT DATE	7a. TOTAL NO. OF PAGES	7b. NO. OF REFS
December 1972	75	19

a. CONTRACT OR GRANT NO.	9a. ORIGINATOR'S REPORT NUMBER(S)
b. PROJECT NO.	
c.	9b. OTHER REPORT NO(S) (Any other numbers that may be assigned this report)
d.	

10. DISTRIBUTION STATEMENT

Approved for public release; distribution unlimited.

11. SUPPLEMENTARY NOTES	12. SPONSORING MILITARY ACTIVITY
	Naval Postgraduate School Monterey, California 93940

13. ABSTRACT

The effect of gravity levels up to 400 times the local gravity value (a/g) was experimentally investigated in a copper, rotating, cylindrical boiler. Heat flux levels up to 80,000 BTU/hr-ft^2 were reached.

Observed improvement in heat transfer at low heat flux values with increasing gravity levels confirmed the results of previous investigations. At high heat flux values, a consistent trend was not observed. With increasing gravity levels, some data indicated a decrease in heat transfer while other data indicated an increase in heat transfer. Changes in heat transfer with variation of the liquid annulus thickness was noted.

DD FORM 1 NOV 68 1473 (PAGE 1)

S/N 0101-807-6811

Security Classification

A-31408

KEY WORDS	LINK A		LINK B		LINK C	
	ROLE	WT	ROLE	WT	ROLE	WT
Nucleate Pool Boiling						
Heat Transfer						
Gravity Effect on Boiling						
Thermosyphon						

141737

Thesis
S5775
c.1

Smith
The effect of gravity on nucleate pool boiling of water.